Available online at www.sciencedirect.com
ScienceDirect
Mechanics of Materials 39 (2007) 513–523
MECHANICS OF MATERIALS
www.elsevier.com/locate/mechmat

A new methodology to delineate the compactive yield cap of two porous sandstones under undrained condition

Sheryl Tembe [a,*], Veronika Vajdova [a,1], Patrick Baud [b], Wenlu Zhu [c], Teng-fong Wong [a]

[a] Department of Geosciences, State University of New York at Stony Brook, 345 ESS Building, Stony Brook, NY 11794-2100, USA
[b] Institut de Physique du Globe (CNRS/ULP), Strasbourg, France
[c] Department of Geology and Geophysics, Woods Hole Oceanographic Institution, USA

Received 14 September 2005; received in revised form 14 July 2006

Abstract

We have developed an experimental methodology to investigate the compactive yield behavior of porous sandstones under undrained condition and to distinguish it from the conventional method we refer to it as "modified undrained". In a conventional undrained test a sample is deformed while the confining pressure and pore volume are fixed. Our novel method is designed to simulate undrained experiments by maintaining a constant pore fluid volume during triaxial loading. However, unlike in typical undrained experiments where pore pressure is allowed to vary, the modified method maintains a constant pore pressure, and instead relies on the simultaneous manipulation of the confining pressure and axial stress to maintain a constant pore fluid pressure. We apply this method to two sandstones precompacted inelastically to a range of porosities. The stress paths from a modified undrained test map out isoporosity stress contours that would coincide with the yield caps, if the elastic strain is negligible. Conventional triaxial experiments under drained condition, in which strain hardening was observed, provide constraints on the yield caps for different values of plastic volumetric strains. While at high mean stresses the yield caps for plastic strains <3% correlate with the isoporosity contours, we observed that at high deviatoric stresses and plastic strains the yield caps diverged from the isoporosity contours. This point of divergence was concomitant with an upsurge of acoustic emissions, implying that the stress path for an undrained experiment has pushed into a stress regime beyond the current yield cap thus triggering inelastic damage.

Keywords: Undrained; Poroelasticity; Strain hardening; Yield cap

1. Introduction

The poromechanical behavior of rocks under "undrained" condition is of fundamental importance in many geologic and geotechnical problems. The stress transfer and triggering of earthquake sequences have been analyzed using poroelastic

* Corresponding author. Tel.: +1 6316328302; fax: +1 6316328240.
E-mail address: stembe@ic.sunysb.edu (S. Tembe).
[1] Now at ReedHycalog, Houston, Texas, USA.

0167-6636/$ - see front matter © 2006 Elsevier Ltd. All rights reserved.
doi:10.1016/j.mechmat.2006.08.005

models that hinge on parameters such as Skempton's coefficient (Roeloffs, 1996; Rudnicki, 2001). It has also been suggested that pore pressure excesses exist in sedimentary formations capped by relatively impermeable layers (Bredehoeft and Hanshaw, 1968) or sealed compartments in active fault zones (Byerlee, 1993), and hence data from undrained experiments provide upper bounds on such pore pressure. Accordingly laboratory studies have been conducted under undrained condition to characterize the poroelastic (e.g. Green and Wang, 1986; Fredrich et al., 1995; Lockner and Stanchits, 2002), plastic and failure (e.g. Ismail and Murrell, 1976; Yassir, 1990) behavior of rocks and sediments.

Laboratory data from an undrained test on a yielding sample can also provide useful constraints on elastic–plastic constitutive models for granular materials. To the extent that the elastic deformation can be considered as negligible relative to the plastic deformation, an undrained experiment in which the pore volume is maintained constant would then involve zero plastic volumetric strain and accordingly the stress path during such an experiment corresponds to a plastic yield envelope (Yu, 1998; McDowell, 2002), assuming that it evolves as a function of only the plastic volumetric strain and not shear strain. Such an analysis can potentially map out a series of yield caps associated with strain hardening in a single undrained experiment, thus avoiding the requirement to perform many triaxial tests under drained condition on multiple samples that may involve appreciable variability.

Conventionally in an undrained experiment the saturated sample is deformed while the confining pressure is maintained constant and drainage of fluid in or out of the pore space is inhibited. While such a boundary condition is easier to implement in a large soil samples with high porosity, it poses significant technical difficulties in a relatively compact rock. If the deformation is compactive then reduction of the pore volume results in an increase of the pore pressure. To ensure that the pore volume remains constant during such a conventional undrained test, it is critical to ensure that the pore pressure system contributes negligible volume and compressibility to the overall mechanical response, or else it should be specially designed so that the system compressibility can be appropriately compensated (Lockner and Stanchits, 2002). To circumvent this difficulty we develop in this study a modified methodology: instead of a fixed confining pressure, the rock sample is deformed while the pore pressure is maintained constant and the confining pressure continually adjusted to maintain the pore volume constant. This has the advantage that one does not need to account for compressibility of the pore pressure system since the pore pressure is constant. To distinguish this experimental methodology from a conventional undrained test, we will refer to it as "modified undrained".

To relate the stress path during an undrained test to the yield caps at different plastic volumetric strains, it is necessary to infer how the total strain is partitioned between the elastic and plastic components. The quantitative characterization of this partitioning in either rock or soil is not straight forward because it is difficult to differentiate unambiguously the two strain components. However, in a porous rock the measurement of acoustic emission (AE) activity can be used to identify the stress states at which plastic strain becomes significant and the stress path is no longer parallel to the current yield cap. Extensive microstructural observations (Menéndez et al., 1996; Wu et al., 2000; Bésuelle et al., 2003) have shown that the dominant micromechanical process for compactive yield in porous sandstones is Hertzian fracture and grain crushing, which are manifested by upsurges in AE activity (Zhang et al., 1990; Wong et al., 1997; Baud et al., 2004), resulting in AE as a powerful diagnostic tool for the onset of damage as a proxy for inelastic yield in rocks (Holcomb and Costin, 1986; Lockner, 1993). If the AE activity is monitored during an undrained test, an upsurge in AE activity would indicate the occurrence of damage and the onset of plastic yield, and the corresponding stress state represents the point at which the stress path begins to significantly deviate and push into the yield cap.

The overall objective of this study is to investigate the compactive yield behavior of two porous sandstones under undrained condition. In many respects the phenomenological behavior and undrained stress path presented here are qualitatively similar to those of normally consolidated clay (Roscoe et al., 1958; Yassir, 1989). Our undrained deformation data were all acquired in modified undrained tests while AE activity was simultaneously monitored. For reference we also include here data from conventional triaxial tests under drained condition, which provide constraints on the initial and subsequent yield caps at different values of plastic volumetric strains. Implications of the experimental data on constitu-

tive modeling of poromechanical behavior and compactive yield of granular materials will be discussed.

2. Experimental procedure

Two sandstones of similar porosity Φ and grain size were selected for this study, the Adamswiller and Diemelstadt sandstones. To be able to compare with the previous study of Wong et al. (1997) we have used Adamswiller sandstone samples cored from the same block and in the same orientation (parallel to sedimentary bedding). The Diemelstadt sandstone samples were cored perpendicular to sedimentary bedding from the same block used by Baud et al. (2004). The petrophysical properties are compiled in Table 1. The samples were cylindrical in shape, with a diameter of 18.4 mm and length of 38.1 mm.

All experiments were conducted at room temperature on jacketed samples saturated with distilled water at a fixed pore pressure of 10 MPa. The pore volume change was recorded by monitoring the piston displacement of the pore pressure generator with a displacement transducer (DCDT), and the porosity change was calculated from the ratio of the pore volume change to the initial bulk volume of the sample with an uncertainty of ±0.1%. The axial load was measured with an external load cell with an accuracy of 1 kN. The displacement was measured outside the pressure vessel with a DCDT mounted between the moving piston and the fixed upper platen. The uncertainty of the axial displacement measurement was 10 μm.

Acoustic emission (AE) activity during the experiments was recorded using a piezoelectric transducer (PZT-7, 5.0 mm diameter, 1 MHz longitudinal resonant frequency) mounted on the flat surface of a spacer attached to the jacketed sample. The AE signals were conditioned by a preamplifier (gain 40 dB, frequency response 1.5–5 kHz). To distinguish events from electric noise, a discriminator was used to check to amplitude and oscillation characteristics of the incoming signal. (See Zhang et al. (1990) for details.)

We will adopt the convention that compressive stresses and compactive strains (i.e., shortening and porosity decrease) are positive and we will denote the maximum and minimum principal compressive stresses by σ_1 and σ_3, respectively. The pore pressure will be denoted by P_P, and the difference between the confining pressure ($P_C = \sigma_2 = \sigma_3$) and pore pressure will be referred to as the *effective pressure* P_{eff}. The mean effective stress $(\sigma_1 + 2\sigma_3)/3 - P_P$ will be denoted by P and the differential stress $\sigma_1 - \sigma_3$ by Q.

Two types of mechanical tests were conducted. In a drained test a saturated sample was hydrostatically loaded to a confining pressure in the range between 20 and 175 MPa, which was then maintained constant while the axial stress was applied in the conventional triaxial configuration. The stress was applied by a servo-controlled hydraulic system at a fixed axial displacement rate, corresponding to a nominal strain rate of $1.0 \times 10^{-5}\ s^{-1}$, which was sufficiently slow to ensure that the deformation was fully drained while the pore pressure generator was continually adjusted to maintain the pore pressure constant at 10 MPa.

The second type of test was designed to simulate undrained experiments by maintaining a constant pore fluid volume during triaxial loading. In our modified undrained test the pore pressure was fixed, in contrast to a conventional undrained experiment which typically allows the pore pressure to vary while maintaining a constant confining pressure. In our approach the pore pressure and pore volume were maintained constant by manually controlling the confining pressure while an increasing axial stress was applied to the sample. In this study we focus on inelastic compaction of porous sandstones, which would tend to decrease the pore volume and in order to counteract this effect the confining pressure was decreased thus allowing the pore volume to increase accordingly.

In a modified undrained experiment the sample would first be loaded hydrostatically to a pressure just beyond the onset of yielding, which typically involves grain crushing and pore collapse in a porous sandstone. The critical pressure P^* at the onset

Table 1
Petrophysical properties of the two sandstones used in this study

Sandstone	Porosity Φ (%)	Grain diameter (mm)	Modal composition
Adamswiller	22.6	0.18	Quartz 71%, feldspar 9%, clay 11%, oxides and mica ~5%
Diemelstadt	24.3	0.16	Quartz 68%, feldspar 26%, oxides 4%, micas 2%

of yield is marked by an inflection point in the hydrostat and upsurge of AE activity (Zhang et al., 1990). The axial stress was then applied at a nominal axial strain rate of $1.9 \times 10^{-5}\ s^{-1}$ while decreasing the confining pressure. Fig. 1 illustrates the evolution of confining pressure and pore volume for a Diemelstadt sandstone sample initially compacted to a confining pressure of 214 MPa. Application of the differential stress induced the sample to compact and pore pressure to increase, and to compensate for the increase in pore pressure, the confining pressure was continually reduced to maintain the pore pressure within ±0.05 MPa of the nominal value of 10 MPa. The fluid drainage associated with this fluctuation in pore pressure may be inferred from our measurement of the volumetric increase of the pore pressure system due to a unit increase in fluid pressure (using a solid sample in place of the porous rock). According to this calibration the system storage was $2.44 \times 10^{-8}\ m^3/MPa$, and therefore the fluctuation of ±0.05 MPa in pore pressure would translate to a pore volume change and fluid drainage from the sample of $\pm 1.22\ mm^3$. Such a volume change would correspond to a porosity fluctuation or equivalently a volumetric strain of ±0.012% for a sample with bulk volume of $10.131\ cm^3$. The drainage in and out of the Diemelstadt sample inferred from the experimental data is also shown in Fig. 1. This modified undrained test was terminated when the confining pressure decreased to 100 MPa.

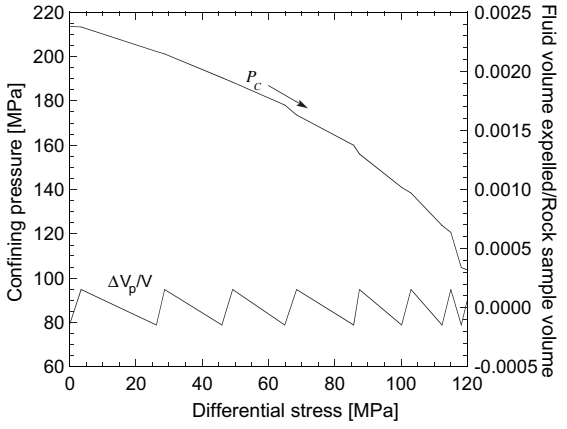

Fig. 1. The stress path in a modified undrained experiment for a Diemelstadt sandstone sample deformed with pore pressure maintained at 10 ± 0.05 MPa. The fluctuation in pore pressure can be attributed to fluid drainage in and out of the saturated sample, which is also shown.

3. Mechanical data of Adamswiller sandstone

3.1. Yield stresses determined from triaxial compression tests under drained condition

Fig. 2 shows data for Adamswiller sandstone deformed in conventional triaxial compression under drained condition. Except for the experiment at effective pressure of 175 MPa which was conducted in this study, the mechanical data were acquired previously by Wong et al. (1997). The top graph in Fig. 2a shows the differential stress versus the axial strain for four experiments at a fixed pore pressure of 10 MPa and with confining pressures maintained at 70, 110, 160 and 185 MPa, respectively. The bottom graph shows porosity decrease versus axial strain for the same samples. In all these experiments strain hardening was observed while the porosity decreased monotonically. Shear localization was not evident in samples deformed to an axial strain of up to 30%.

Fig. 2b shows the effective mean stress as a function of the porosity change for the drained experiments. For reference the curve for hydrostatic loading from Wong et al. (1997) is also included as the dashed curve. Typically for a porous sandstone such a hydrostat shows an inflection point (marked as P^* in Fig. 2b) which, according to microstructural and AE measurements, corresponds to the critical effective pressure for the onset of grain crushing and pore collapse (Zhang et al., 1990). In a triaxial compression experiment the nonhydrostatic and hydrostatic loadings are coupled. If the axial stress increases by an increment $\Delta\sigma_1$ while the confining and pore pressures are maintained constant, then the effective mean stress P and differential stress Q would increase by the amounts $\Delta\sigma_1/3$ and $\Delta\sigma_1$, respectively. If the porosity change is elastic, then it is solely controlled by the hydrostatic stresses and independent of the differential stress, and therefore the triaxial data (solid curves) in Fig. 2b should coincide with the hydrostat (dashed curve). Any deviation from the hydrostat would imply that the porosity change in a triaxial compression experiment depends on not only the effective mean stress, but also the deviatoric stresses. This in turn implies the onset of inelastic yield. In each experiment shown in Fig. 2b the triaxial curve for a given effective pressure coincided with the hydrostat up to a critical stress state (indicated by C^* for the experiment at 100 MPa effective pressure), beyond which there was an accelerated decrease in porosity in

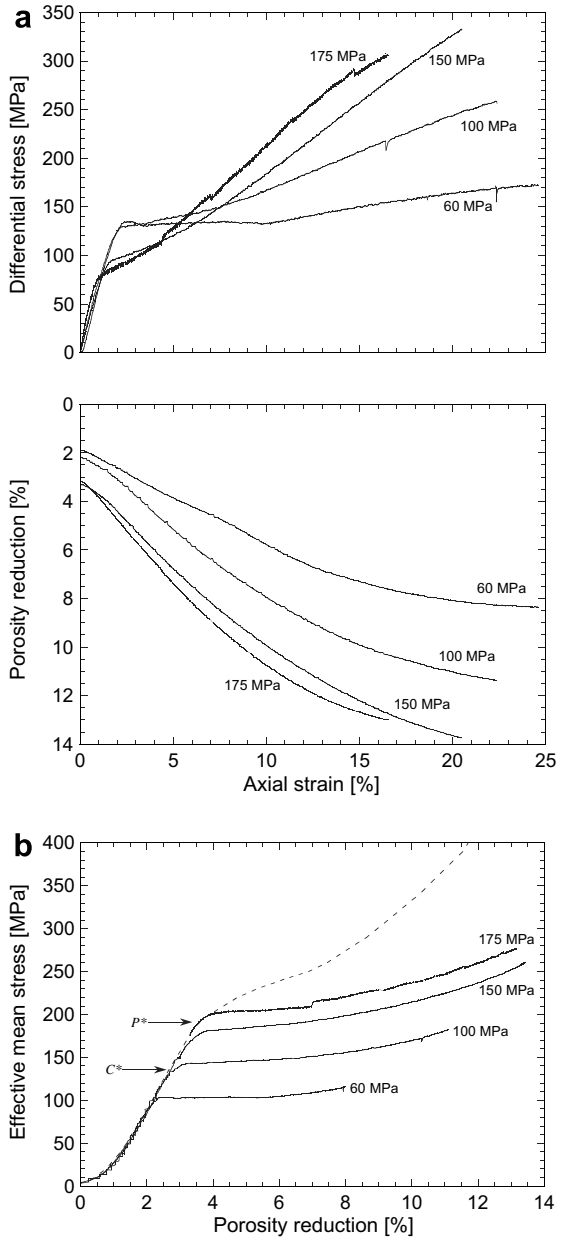

Fig. 2. Drained experiments on Adamswiller sandstone samples deformed in conventional triaxial compression with 10 MPa pore pressure at the effective pressures indicated. The experiment at 175 MPa is from this study. All others are from Wong et al. (1997). (a) Differential stress and porosity reduction as functions of axial strain. (b) Effective mean stress as a function of porosity reduction. The critical stress for the onset of shear-enhanced compaction C^* is the point where the triaxial experiment deviates from the hydrostat. The grain crushing pressure P^* for Adamswiller is also indicated.

comparison to the hydrostat. At stress levels beyond C^* the deviatoric stress field provided significant contribution to the compactive strain, and this phenomenon of inelastic yield by "shear-enhanced compaction" (Curran and Carroll, 1979; Wong et al., 1997) is attributed to the inception of grain crushing and pore collapse in the sandstone (Menéndez et al., 1996).

These data for P^* and C^* from drained tests at fixed confining pressures represent the initial yield stresses, which are shown in Fig. 3 as the solid circles in the $P-Q$ stress space. Wong et al. (1997) concluded that the initial yield stresses at the onset of shear-enhanced compaction are in good agreement with an elliptic cap of the form

$$\frac{(P/P^* - \gamma)^2}{(1-\gamma)^2} + \frac{(Q/P^*)^2}{\delta^2} = 1 \tag{1}$$

Their data for seven sandstones with porosities ranging from 14% to 35% were observed to fit elliptic caps with $\gamma \sim 0.5$ and δ ranging from 0.5 to 0.7.

If the strain hardening behavior observed in drained experiments is characterized by a yield function that depends solely on the plastic volumetric strain, then subsequent yield caps can be mapped as contours in the stress space corresponding to specific values of plastic volumetric strain ε_v^p. Since plastic deformation of the solid grains in a sandstone is negligible at room temperature under the pressure conditions in our experiments, the plastic porosity change $\Delta\Phi^p$ represents the bulk of the plastic volumetric strain, and to a first approximation $\varepsilon_v^p = \Delta\Phi^p$ (with the convention that $\Delta\Phi^p$ is positive

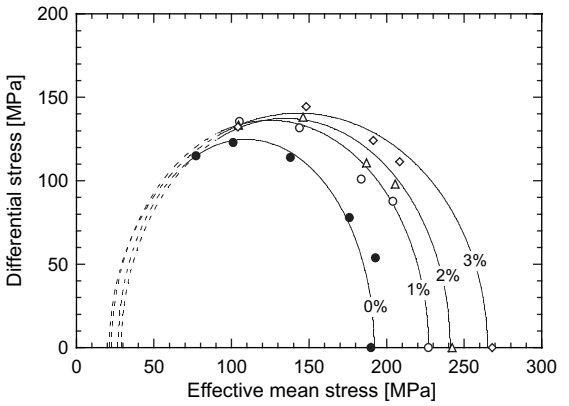

Fig. 3. The yield stresses C^* associated with the onset of shear-enhanced compaction for the drained experiments (dark circles) map out the initial yield cap for Adamswiller sandstone. Similarly, yield caps for plastic volumetric strains of 1% (open circles), 2% (triangles) and 3% (diamonds) can be mapped out. The yield loci are fitted by an elliptical cap (Eq. (2)) that represent plastic strain contours (solid lines) (Baud et al., in press).

for compaction). From a plot of the total porosity change versus effective mean stress (Fig. 2b) the plastic porosity change $\Delta\Phi^{p}$ at a given point beyond C^{*} was evaluated by subtracting the elastic porosity change, which is assumed to be given by the linear portion during the initial loading, from the total porosity change Df. We plot in Fig. 3 the yield stresses attained in the four drained tests at constant values of ε_{v}^{p} ranging from 0.01 to 0.03.

In a recent study of such yield data for four sandstones, Baud et al. (in press) concluded that both the initial and subsequent yield stresses can be described by elliptic caps. Specifically for the Adamswiller sandstone they concluded that the data fit quite well elliptic caps of the form

$$\frac{(P-C)^2}{A^2}+\frac{Q^2}{B^2}=1 \qquad (2)$$

with semi-axes A and B and center at $(C,0)$. These three parameters are functions of ε_{v}^{p}, and up to a plastic volumetric strain of 0.03. These four elliptic caps are shown as solid curves in Fig. 3.

3.2. Isoporosity stress contours from modified undrained tests

We present in Fig. 4a the data for a sequence of five modified undrained experiments conducted on one Adamswiller sandstone sample with starting porosity of 22.6%. This sample was initially compacted hydrostatically to an effective pressure of 203 MPa ($>P^{*}=190$ MPa), thus reducing the porosity to a value of 20% and incurring a volumetric strain of 2.6%. The axial stress was then applied, and to maintain the porosity and pore pressure constant the confining pressure was continually reduced to attain a final value of 90 MPa. The axial load was then released, maintaining the confining pressure constant at 90 MPa and pore pressure at 10 MPa.

In the second run the sample was hydrostatically compacted further, reducing the porosity to 18.2%. The axial loading was then applied, again reducing continually to maintain the pore pressure and volume constant. We terminated the axial loading at a confining pressure of 115 MPa, after which the axial load was released keeping the confining pressure constant at this value. These processes were repeated in three subsequent runs at porosities of 16.8%, 15.5% and 14.2% (Fig. 4a).

We plot in Fig. 4b the stress paths traversed in these five tests. Since they represent stress states at constant porosity we refer to them as "isoporosity stress contours". For comparison we also show here the initial yield stresses determined from the drained tests. The overall agreement implies that the isoporosity stress contours can provide complementary

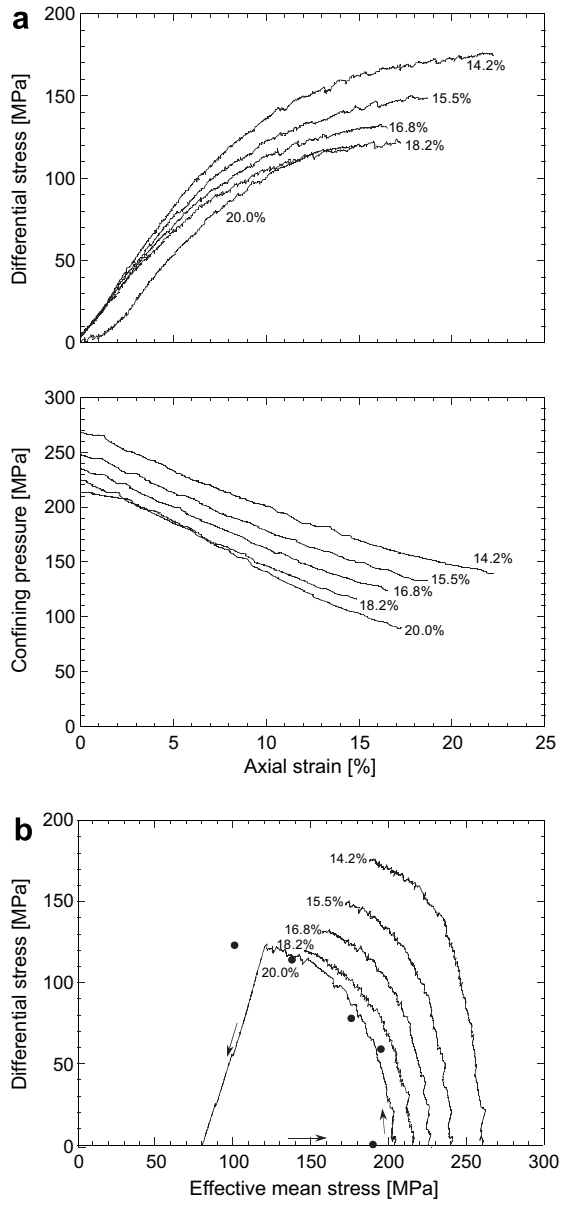

Fig. 4. A sequence of five modified undrained experiments on Adamswiller sandstone sample Bun 28 with an initial porosity of 22.6%. The porosities were maintained constant at the values indicated. The first undrained test was conducted at a porosity of 20.0%, and subsequent tests at decreasing values of porosity. (a) Differential stress and confining pressure as functions of axial strain. (b) Isoporosity stress contours from undrained tests, and for comparison the initial yield stresses (dark circles) from drained experiments. The arrows indicate the stress path direction for an undrained experiment.

data on the yield caps, especially in the stress regime with relatively high mean stresses close to the hydrostatic yield stress P^*. There is a missing "gap" in the yield data from drained tests (Fig. 3) in this stress regime where the yield stress rises rapidly with slight decrease of mean stress, and therefore it is difficult to fill in this gap unless one conduct numerous duplicate experiments at confining pressures very close to P^*. However, there is an overall trend for the yield caps at higher plastic strains shown in Fig. 3 to deviate from the corresponding isoporosity contours, especially in the regime with higher differential stresses and lower mean stresses. This implies that at some point in a modified undrained test the isoporosity stress path crossed the current yield envelope, pushing into a stress regime favorable for the development of additional inelastic damage.

Indeed our AE measurements seem to support this interpretation. Compactive damage in a porous sandstone typically involves grain crushing which would generate a large number of AE events (Zhang et al., 1990; Wong et al., 1997). We show in Fig. 5a the cumulative number of AE events recorded along the isoporosity stress contour for the undrained test at porosity of 20%. Relatively little AE activity was observed along the contour for most of the experiment, which implies that little damage was sustained and the stress contour approximates the yield cap up to a differential stress of ~113 MPa when an upsurge in AE was observed. In Fig. 5b we plot the stress levels at which AE upsurges were observed in all five undrained experiments. These are all located in a regime with relatively high differential stresses, and also where a comparison with the yield stresses determined from the drained tests indicate discrepancy between yield stresses and isoporosity contours (Fig. 4b).

Since we maintained the porosity constant, the plastic volumetric strain ($\Delta\varepsilon_v^p \approx \Delta\Phi^p$) accumulated at the stress state where the cross over occurred can be estimated by what was necessary to counteract the elastic porosity increase ($\Delta\varepsilon_v^e$) due to the reduction of confining pressure. For the experiment shown in Fig. 5a, the effective mean stress P dropped by $\Delta P \approx 50$ MPa from the initial value of 203 MPa to stress state at the upsurge of AE activity. The pore compressibility $\beta_\phi = (1/\phi)(\partial\phi/\partial P)$ for Adamswiller sandstone deformed under similar conditions was estimated to be 10^{-3} MPa^{-1} (Wong et al., 1997). Hence the elastic dilation $\Delta\varepsilon_v^e$ can be estimated as $\phi\beta_\phi\Delta P = 0.01$, which would be balanced by a compactive strain $\Delta\varepsilon_v^p = 0.01$ to maintain the porosity constant at 20%. Similar estimates were made for the other four experiments shown in Fig. 5b, which range from 0.004 to 0.01.

4. Mechanical data of Diemelstadt sandstone

4.1. Variability of mechanical behavior

In our inference of yield stresses from multiple drained tests at different effective pressures, it is implicitly assumed that the variability of mechanical behavior from sample to sample is small. Indeed the reproducibility of mechanical behavior in Adamswiller sandstone is such that drained tests provide a consistent set of data for the yield caps (Fig. 3). In contrast the mechanical behavior in Diemelstadt

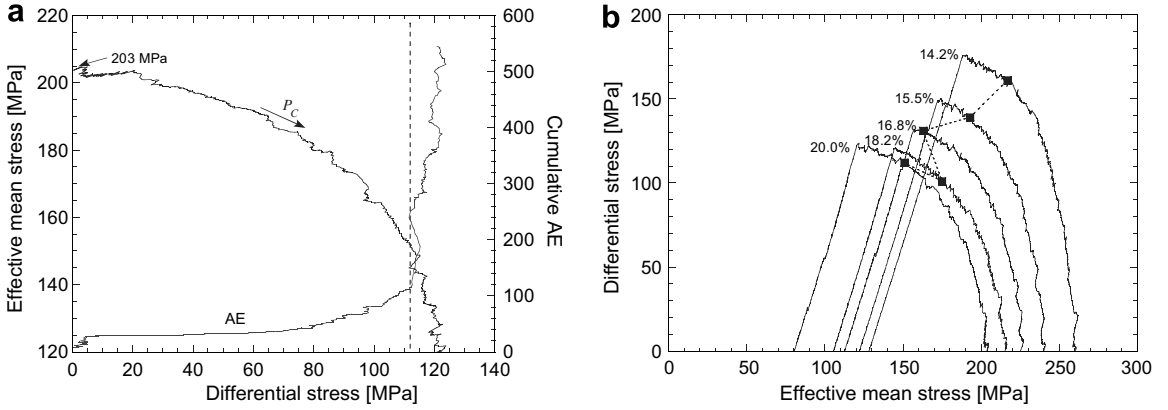

Fig. 5. (a) Effective mean stress and cumulative AE counts as functions of differential stress in a modified undrained experiment on Adamswiller sample Bun 28. The dashed line marks the point in the stress space associated with an upsurge in AE. (b) The stress states associated with an upsurge in AE are shown as dark squares on the isoporosity stress contours for the five undrained experiments.

sandstone is highly variable from sample to sample. Although our samples were from the same block, there is a subset of cores that had initial heterogeneities in the form of relatively thin bedding laminae. Fig. 6 shows our data for duplicate experiments on two Diemelstadt sandstone samples deformed at the same confining pressure of 140 MPa and pore pressure of 10 MPa under drained condition. Although both show overall strain hardening, the differential stresses and porosity reduction attained at the same axial strain were appreciably different in the two samples.

We conducted a total of 12 drained experiments, including four sets of duplicate experiments at effective pressures of 80 MPa, 110 MPa, 130 MPa and 150 MPa. The sample-to-sample variability is significant, as shown in Fig. 7 which compiles all the data for the initial yield stresses C^* (the dark circles). Not surprisingly the undrained behavior was also variable, as illustrated in the same figure by the isoporosity stress contours for three samples initially hydrostatically compacted to just beyond the critical pressure P^*. Notwithstanding the variability from sample to sample, the drained and undrained data are consistent in the sense that most of the drained data for initial yield stresses are bracketed by the isoporosity contours, except in the regime with high differential stresses and low mean stresses.

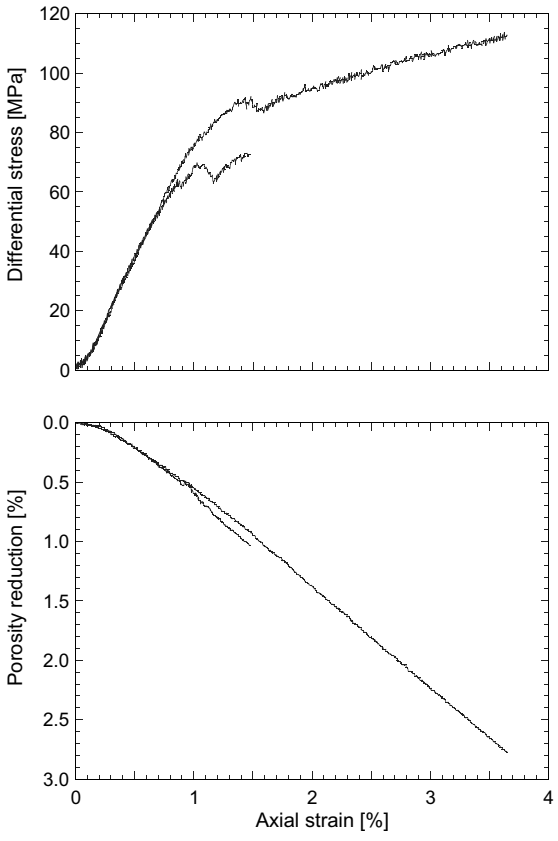

Fig. 6. Duplicate drained experiments of Diemelstadt sandstone deformed at a confining pressure of 140 MPa and 10 MPa of pore pressure. As functions of axial strain, the differential stress and porosity reduction were appreciably different in the two experiments.

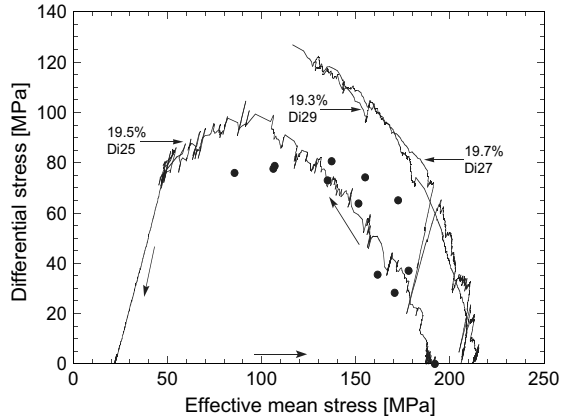

Fig. 7. The variability between Diemelstadt sandstone samples is apparent in scattering of the initial yield stresses C^* (dark circles) for drained experiments. The isoporosity stress contours also reflect this variability in the three undrained experiments compacted just beyond P^*, which bracket the drained data.

4.2. Evolution of yield stresses inferred from isoporosity stress contours

Since it is not feasible in the case of Diemelstadt sandstone to determine the evolution of yield stresses from drained experiments at different effective pressures, we will use isoporosity stress contours from a sequence of undrained experiments conducted on the same sample to infer the development of the yield cap with strain hardening. The Diemelstadt sample Di29 was initially compacted hydrostatically to an effective pressure of 204 MPa ($>P^* = 195$ MPa), thus reducing the porosity to a value of 19.3%. The differential stress and confining pressure as functions of axial strain in this first test, as well as those for four subsequent undrained tests (at constant porosities of 17.6%, 15.5%, 13.4% and 12.1%) are shown in Fig. 8a. The isoporosity stress contours are shown in Fig. 8b, and for comparison the initial yield stresses from drained experiments are also shown.

The geometric shape of the stress contours is qualitatively similar to that of Adamswiller sand-

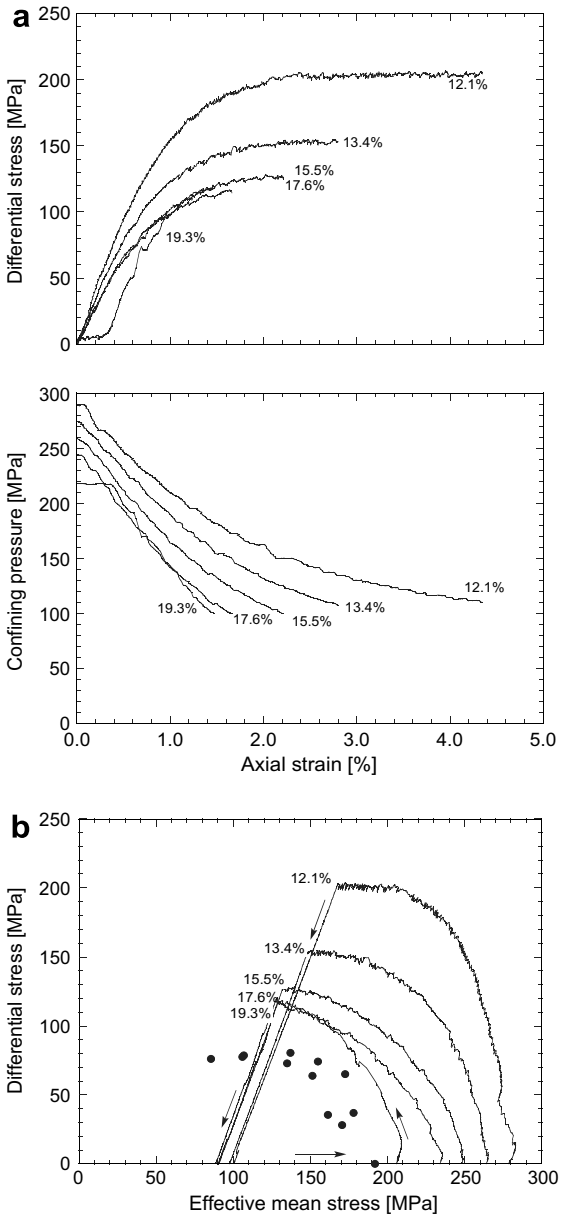

Fig. 8. A sequence of five modified undrained experiments on Diemelstadt sandstone sample Di 29. The porosities were maintained constant at the values indicated. The first undrained test was conducted at a porosity of 19.3%, and subsequent tests at decreasing values of porosity. (a) Differential stress and confining pressure as functions of axial strain. (b) Isoporosity stress contours from undrained tests, and for comparison the initial yield stresses (dark circles) from drained experiments. The arrows indicate the stress path direction for an undrained experiment.

stone. The strain hardening was manifested by horizontal translation and expansion of the contours. To estimate the stress levels at which damage became appreciable we also conducted AE measurements. Fig. 9a shows the cumulative number of AE events recorded along the isoporosity stress contour for the undrained test at porosity of 13.4%. Relatively little AE activity was observed along the contour up to a differential stress of ~138 MPa when an upsurge in AE was observed. In Fig. 9b we plot the stress levels at which AE upsurges were observed in the five undrained experiments. Similar to Adamswiller sandstone (Fig. 5b) these critical stresses are all located in a regime with relatively high differential stresses. We determined the pore compressibility to be $8 \times 10^{-14}\,\mathrm{MPa}^{-1}$, and the plastic volumetric strain accumulated at these stress states to range from 0.003 to 0.01.

5. Discussion

In this study we develop an experimental methodology for investigating the mechanical behavior of porous rocks under undrained condition. It was applied to two porous sandstones undergoing compactive yield. The stress paths in such a modified undrained test provide data complementary to these from drained tests for the yield caps especially in the stress regime with relatively high mean stress and low differential stress. This is the regime in which the yield stress rises rapidly with slight decrease of mean stress, rendering it difficult to determine the yield behavior from conventional triaxial tests under drained condition. Mechanical data from drained tests showed that the normality condition may apply in this stress regime (Wong et al., 1997), and therefore the associated flow rule can be used if the yield cap is known. Another reason for obtaining better constraints on the yield caps in this regime is that bifurcation analyses of the onset of strain localization in porous sandstone have shown that the development of shear and compaction bands is very sensitive to the cap shape at relatively high mean stresses (Rudnicki, 2004).

Our data for the Diemelstadt sandstone also demonstrate that the methodology can provide pertinent information on the development of yield behavior with strain hardening in a rock that is highly variable in its mechanical behavior. It is likely that a similar methodology can be applied to the study of yield and failure in other porous rocks and granular materials. Our approach was developed with compactant yield in mind. In these experiments the pore volumes of the samples decrease with deformation. However, it should be noted that under lower confinement, the failure of

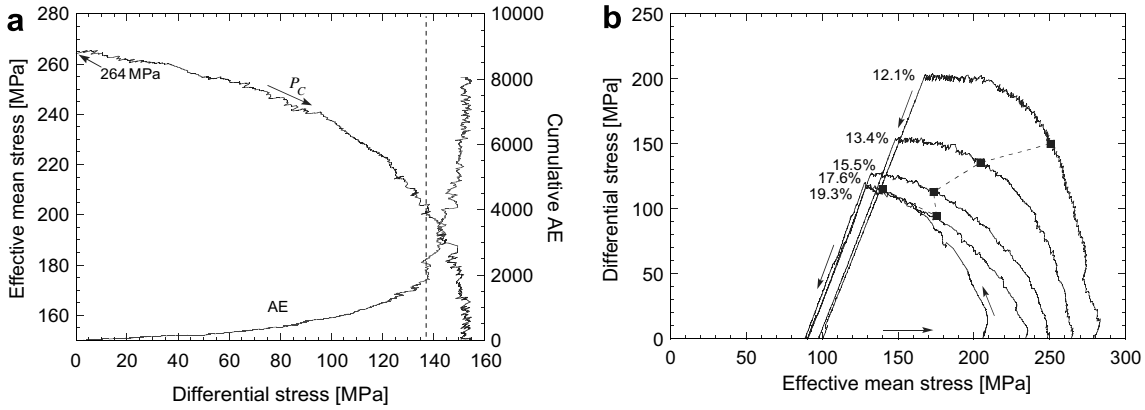

Fig. 9. (a) Effective mean stress and cumulative AE counts as functions of differential stress in a modified undrained experiment on Diemelstadt sandstone sample Di 29 (23.7% initial porosity). The dashed line marks the point in the stress space associated with an upsurge in AE. (b) The stress states associated with an upsurge in AE are shown as dark squares on the isoporosity stress contours for the five undrained experiments.

rock or soil typically involves dilatancy and shear localization for which our methodology will not be directly applicable.

The use of AE measurement to monitor the onset of damage in an undrained test proved to be useful in constraining the stress level at which an isoporosity stress contour would cross over the current yield cap. This cross-over typically occurs in a regime with relatively high differential stresses and low mean stresses, where the failure mode in a porous sandstone undergoes the transition from ductile flow to brittle faulting (Menéndez et al., 1996; Baud et al., 2004). In this transitional regime the normality condition is not applicable, as shown by the recent study of Baud et al. (in press) of yield behavior in four porous sandstones. Our data here imply that the isoporosity stress contours in this regime tend to overestimate the yield stresses, but even if the undrained data were to provide good approximations to the yield stress they would not be sufficient for predicting the plastic yield behavior since it is necessary to incorporate a non-associated flow rule here.

Acknowledgements

We have benefited from discussions with Eric Grueshow, Laurent Louis, and John Rudnicki. We also thank the two anonymous reviewers for their thoughtful comments. The first modified undrained experiment was initiated by Wenlu Zhu during her visit at SUNY Stony Brook. Financial support for WZ was provided by NSF under grant EAR-0510459 and Department of Energy under grant DE-FG02-06ER15058. ST was supported by a Department of Education GAANN Fellowship. The research at Stony Brook was partially supported by the Office of Basic Energy Sciences, Department of Energy under grant DE-FG02-99ER14996.

References

Baud, P., Klein, E., Wong, T.-F., 2004. Compaction localization in porous sandstones: spatial evolution of damage and acoustic emission activity. J. Struct. Geol. 26, 603–624.

Baud, P., Vajdova, V., Wong, T.-F., in press. Shear-enhanced compaction and strain localization: inelastic deformation and constitutive modeling of four porous sandstones. J. Geophys. Res.

Bésuelle, P., Baud, P., Wong, T.-F., 2003. Failure mode and spatial distribution of damage in Rothbach sandstone in the brittle-ductile transition. Pure Appl. Geophys. 160, 851–868.

Bredehoeft, J.D., Hanshaw, B.B., 1968. On the maintenance of anomalous fluid pressures. I: Thick sedimentary sequences. Geol. Soc. Am. Bull. 79, 1097–1106.

Byerlee, J., 1993. Model for episodic flow of high-pressure water in fault zones before earthquakes. Geology 21, 303–306.

Curran, J.H., Carroll, M.M., 1979. Shear stress enhancement of void compaction. J. Geophys. Res. 84, 1103–1112.

Fredrich, J.T., Martin, J.W., Clayton, R.B., 1995. Induced pore pressure response during undrained deformation of tuff and sandstone. Mech. Mater. 20, 95–104.

Green, D.H., Wang, H.F., 1986. Fluid pressure response to undrained compression in saturated sedimentary rock. Geophysics 51, 948–956.

Holcomb, D.J., Costin, L.S., 1986. Detecting damage surfaces in brittle materials using acoustic emissions. J. App. Mech. 108, 536–544.

Ismail, I.A.H., Murrell, A.F., 1976. Dilatancy and the strength of rocks containing pore water under undrained conditions. Geophys. J. R. Astr. Soc. 44, 107–134.

Lockner, D.A., 1993. The role of acoustic emission in the study of rock fracture. Int. J. Rock Mech. Mining Sci. Geomech. Abstr. 30, 883–899.

Lockner, D.A., Stanchits, S.A., 2002. Undrained poroelastic response of sandstones to deviatoric stress change. J. Geophys. Res. 107 (B12), 2353. doi:10.1029/2001JB00146.

McDowell, G.R., 2002. A simple non-associated flow model for sand. Granular Matter 4, 65–69.

Menéndez, B., Zhu, W., Wong, T.-F., 1996. Micromechanics of brittle faulting and cataclastic flow in Berea sandstone. J. Struct. Geol. 18, 1–16.

Roeloffs, E., 1996. Poroelastic techniques in the study of earthquake-related hydrologic phenomena. In: Dmoska, R., Saltzman, B. (Eds.), Advances in Geophysics, vol. 37. Academic, San Diego, pp. 135–195.

Roscoe, K.H., Schofield, A.N., Wroth, C.P., 1958. On the yielding of soils. Geotechnique 8, 22–53.

Rudnicki, J.W., 2001. Coupled deformation–diffusion effects in the mechanics of faulting and failure of geomaterials. Appl. Mech. Rev. 54, 483–502.

Rudnicki, J.W., 2004. Shear and compaction band formation on an elliptic yield cap. J. Geophys. Res. 109, B03402. doi:10.1029/2003JB002633.

Wong, T.-F., David, C., Zhu, W., 1997. The transition from brittle faulting to cataclastic flow in porous sandstones: mechanical deformation. J. Geophys. Res. 102, 3009–3025.

Wu, X.Y., Baud, P., Wong, T.-F., 2000. Micromechanics of compressive failure and spatial evolution of anisotropic damage in Darley Dale sandstone. Int. J. Rock Mech. Min. Sci. 37, 143–160.

Yassir, N.A., 1989. Undrained shear characteristics of clay at high total stresses. In: Maury, V., Fourmaintraux, D. (Eds.), Rock at Great Depth. A.A. Balkema, Rotterdam, The Netherlands, pp. 907–913.

Yassir, N.A., 1990. The undrained shear behaviour of fine-grained sediments. In: Knipe, R.J., Rutter, R.H. (Eds.), Deformation Mechanisms, Rheology and Tectonics, vol. 54. Geol. Society Special Publication, London, pp. 99–404.

Yu, H.S., 1998. CASM: A unified state parameter model for clay and sand. Int. J. Numer. Anal. Meth. Geomech. 22, 621–653.

Zhang, J., Wong, T.-F., Yanagidani, T., Davis, D.M., 1990. Pressure-induced microcracking and grain crushing in Berea and Boise sandstones: acoustic emission and quantitative microscopy measurements. Mech. Mater. 9, 1–15.